Silicon (2023) 15:7171–7181
https://doi.org/10.1007/s12633-023-02563-8

RESEARCH

Experimental Silica-based Bioceramic Composite Added with Nano-sized Bovine Hydroxyapatite: Synthesis and Characterization

Brunna Mota Ferrairo[1] · Victor Mosquim[2] · Lucas José de Azevedo-Silva[1] · Luara Aline Pires[2] · David Santos Souza Padovini[3] · Aroldo Geraldo Magdalena[3] · Carlos Alberto Fortulan[4] · Paulo Noronha Lisboa-Filho[5] · José Henrique Rubo[1] · Ana Flávia Sanches Borges[2]

Received: 19 January 2023 / Accepted: 10 June 2023 / Published online: 28 June 2023

Abstract

Purpose To produce an experimental dense silica-based bioceramic composite added with nano-sized hydroxyapatite (HA) for biomedical application and physicochemical/ microstructurally characterize varying the firing temperature and the amount of binder, polyvinyl butyral (PVB).

Methods Fumed SiO_2 and nano-sized HA powder from bovine bone were ball milled aiming the mixture of powders. Groups were divided into HA (3, 5 and 10%), and PVB (1.2 and 2.4 wt.%) addition, and sintering process (1100, 1200 and 1300 °C with a 4 h plateau). The materials were characterized by X-ray Diffraction (XRD), Fourier Transform Infrared (FTIR) and Scanning Electron Microscopy (SEM) with Energy Dispersive X-ray Spectroscopy analysis (EDX).

Results The group fired at 1200 °C presented potentialized chemical bonds without the degradation of HA at XRD profile, based on its microstructural evolution. FTIR spectra shows the degradation of HA, with an increase of CO_2 band and a loss of the calcium-phosphate bands as the temperature increases. The binder concentration showed no chemical changes in the material. 2.4 wt.% of PVB addition resulted in optimized compaction and a lower inclusion of pores or cracks, suggested by SEM images.

Conclusion This study suggests that the match composition of SiO_2 matrix with 5% of HA and 2.4 wt.% of PVB, sintered at 1200 °C, exhibit potentially superior properties to biomaterial applications.

Keywords Ceramic material · Nanoparticles · Nanostructured materials · Silica · Hydroxyapatite · Composite ceramics

1 Introduction

Studies about synthesis of bioceramics has been detached due to its wide applicability in orthopedics and dentistry reconstructing and repairing musculoskeletal system. Silicon is often present in bioceramics composition because it is an important micronutrient for bone and connective tissue health [1, 2], participating in the early stages of bone mineralization by directly stimulating and upregulating osteoblasts proliferation [3–5] and gene expression [6]. High concentrations ($\geq$ 30–50 wt.% of SiO_2) have been investigated and perform surface reactions on initial cellular and ionic process, allowing the crystallization of apatite crystals, collagen formation and cell adhesion [7].

Hydroxyapatite [$Ca_{10}(PO_4)_6(OH)_2$] (HA) is thermodynamically stable in its crystalline state in body fluid and has a special chemical composition that is morphologically

✉ Ana Flávia Sanches Borges
afborges@fob.usp.br

1 Department of Prosthodontics and Periodontics, Bauru School of Dentistry, University of São Paulo, Bauru, SP, Brazil

2 Department of Operative Dentistry, Endodontics and Dental Materials, Bauru School of Dentistry, University of São Paulo, Alameda Dr. Octávio Pinheiro Brisolla, 9-75, Vila Universitária, Bauru, São Paulo 17012-901, Brazil

3 Department of Chemistry, School of Sciences, São Paulo State University, Bauru, SP, Brazil

4 Department of Mechanical Engineering, São Carlos School of Engineering, University of São Paulo, São Carlos, SP, Brazil

5 Department of Physics, School of Sciences, São Paulo State University, Bauru, SP, Brazil

and structurally similar with the mineral portion of human's bone [8]. Bovine bone has the benefit of an easily available and inexpensive source associated with Ca/P ratio, particles shapes and crystalline phases favorable to use as bioactive material [9]. Bioactivity and osteoconductive properties coexist with insufficient mechanical properties for monolithic load-bearing use [10].

The association between Si-HA enhaced for bone formation [7, 11] and attachment [12], and long-term Si delivery system [13] are promising characteristics of this association in different arrangements, e.g., granules [14], microspheres [15], plasma-sprayed coatings [7], scaffolds [16], porous [17] and dense bioceramics [18]. Although the association Si-HA has been much discussed, there is a gap in the literature regarding the densified conformation with silica matrix and HA acting as its additive. Sintering temperature, timing and atmosphere, powder grain size and shape, pressure, composition and manufacture processes are some factors that influence on dense ceramics preparation [19, 20].

Considering the obstacles at reaching proper composition, particle size, synthesis process, microstructural and physicochemical properties, idealizing an experimental material combining SiO_2 and HA (SH composite ceramic) would be remarkable. SH could present a high bioactivity through the release of dissolution ions such as Si, Ca and P, which may also affect vascularization, gene expression in an osteogenic cell, and consequently improve bone formation [21, 22]. Therefore, since high silicon material associated with HA has been produced by different processing methods and achieved interesting results, the aim of this study was to produce a new glass ceramic containing SiO_2/HA via uniaxial/isostatic powder compression and structurally and chemically characterize this material, varying the sintering temperatures and concentration of binder.

2 Materials and Methods

2.1 Nano-sized HA

HA was obtained from bovine femurs. The nanoparticulation process was performed with the aid of a ball mill [23].

2.2 Synthesis of Experimental Material

For the matrix of the experimental material, fumed silica (SiO_2, Sigma-Aldrich) was used, with particle size of 0.007 µm, surface area of 395 ± 25 m^2/gram and apparent density of 2.3 lb./cu. Ft (0,037 g/cm^3). The study variables were (1) the percentage of HA addition (3, 5 and 10%), (2) the temperature of the sintering plateau (1100, 1200 and 1300 °C), and (3) the concentration of PVB (1.2 and 2.4 wt%) (Sigma–Aldrich, USA).

The mixing of the experimental material was mechanically carried out in a ball mill. Considering the molecular weight of amorphous SiO_2 is 2.2 g/cm^3 and of HA is 3.156 g/cm^3, the same jug (100 cm^3 of useful volume) was loaded with 500 g of griding elements (spheres of 3Y zirconia ∅ 10 mm), 30 cm^3 of powder (SiO_2 + HA), 70 cm^3 of isopropyl alcohol (Sigma–Aldrich, USA) and paraminobenzoic acid (PABA, Sigma–Aldrich, USA, 0.05 wt.% over powder wight,), and was placed for 2 h in a rotatory ball mill. After this period, 1.2% or 2.4 wt.% of PVB, previously diluted in isopropyl alcohol, was added to the jug and mixed and homogenized in a rotary ball mill for 10 min.

The content was oven dried at approximately 80 °C and granulated in stainless steel sieves (# 200 mesh ≤ 75 µm). The powder was portioned and pressed in a uniaxial press (100 MPa / 30 s), with the aid of a matrix that was lubricated with a thin layer of oleic acid ($C_{18}H_{34}O_2$, Êxodo Científica, Brazil). Once compacted, the specimens were vacuum packed and received the second pressing in an isostatic press (200 MPa / 1 min).

The SH composite ceramic samples were sintered in atmosphere air by a chamber-type oven (Lindberg Blue / M). Sintering scheme: from room temperature to 160 °C with a heating rate of 2.7° C / min, then to 600° C to 4 °C / min, then up to 1100 °C at 5° C / min and finally up to the maximum temperature (1100, 1200 or 1300 °C) at 6 °C / min, with a 120-min plateau followed by cooling the oven to room temperature.

2.3 Characterization Methods

Four different investigative methodologies were used to chemical and structurally characterize the samples: X-ray diffraction (XRD), Fourier transform infrared (FTIR), scanning electron microscopy (SEM) and energy dispersive X-ray spectroscopy (EDX). They were performed on the initial powders, the blend of powders prior to sinterint process (initial characterization) and the pellets after sintering (final characterization), aiming to compare them and observe the changes caused by sintering and variations in the concentration of HA and PVB.

2.3.1 SEM/EDX

The samples were gold-coated at ≅ 10 nm thickness and investigated using an, on an ultra-vacuum system (base pressure of 1×10^{-5} Pa and acceleration voltage of 20 kV, XL30 FEG). Images were taken (JEOL-JSM 56000LV microscope, Tokyo-Japan), and chemically analyzed with an X-ray detector (Voyager, Noran Instruments).

2.3.2 XRD

Samples were submitted to X-ray diffraction on a diffractometer (Rigaku Miniflex600 X-ray) using CuKα radiation source (λ = 1.54056 Å) with rotatory anode operation at 40 kV and 150 mA. Counting time 0.3 s and scanning angle ranging from 10 to 80°.

The amorphous characteristic of the fumed silica powder and the crystalline phases of HA were identified and validated by XRD. In order to propose standards and evaluate the profiles, the Joint Committee on Powder Diffraction and Standards (JCPDS) was used. Some of the cards selected was: # 29-0085 for amorphous SiO_2, # 024-0033 for HA, # 009-0080 for $CaHPO_4$, # 001-1160 for CaO, and # 001-0941 for $Ca_3(PO_4)_2$.

2.3.3 FTIR

Spectra were recorded using KBr pellets (FTIR-Vertex 70, Bruker), in the transmittance mode with the range of 500–2500 cm^{-1}, in order to investigate the functional groups of resultant powders.

3 Results and Discussion

3.1 Silica and HA Powder Characterization

The use of fumed silica for the experimental ceramics was motivated by the submicron-sized of its particles (like flakes). The smaller the particles, the larger the estimated surface area. This correlation results in a larger area available for interaction with nano-HA and the unique particle flocs promote a dispersion to mechanical stress [24]. The alcoholic medium was attempted to not exceed the threshold concentration (P_g) because the viscous liquid characteristic is beneficial for the ball-mill method making the dilute dispersion flowable when perturbed by mechanical action [25]. Associate fumed silica and polar organic solvents tends to form low viscosities medium and networks of overlapping agglomerates and clusters [24, 26]. Hydrogen bonding between silanol groups on different particle surfaces are caused by the attractive interactions between particle aggregation and network formation [26, 27].

Bovine bone is a well-studied natural source of HA with predictable and reliable characteristics [9]. Due to the structural and morphological similarity with the human bone, the cortical portion of the femur was chosen for the study [28]. The pre-treatment step removed the collagen, lipids and non-collagenous proteins organic from the bone matrices [29] and if any residue remained, it was burned during calcination at 900º, remaining only the mineral phase (HA).

XRD analysis of the silica fumed and HA as shown in Fig. 1 exhibited peaks within the 2θ range from 10° to 80° that corresponds to stoichiometric of the amorphous structure of SiO_2 (JCPDS no. 29-0085) and HA (JCPDS no. 9-432). No phase decomposition (CaO, TTCP, a-TCP and b-TCP) was found and it can be observed the high crystallinity and single phase on HA spectra of starting powder. This finding highlight that the sintering treatment produced pure HA.

The IR spectrum of starting powders coincide with those described in the literature. Silica fumed presents the vibration of Si-O-Si and Si-OH bands while the inorganic phase of HA is composed mainly of Ca and P with some minor components (O, C, Na, and Mg) [30]. Spectrum of HA shows the presence of major inorganic species, phosphate (from the mineral HA), carbonate (from carbonate substitution for hydroxyl and phosphate groups in HA), and organic components such as amide functional groups I–III from the bone protein constituents (mainly type I collagen) (Fig. 2) [31].

3.2 SH Composite Ceramic Conception

3, 5 and 10% of nano-HA were selected based on previous studies with silica-based ceramics that receive the addition of crystalline material, such as ZrO_2 [32, 33], and studies

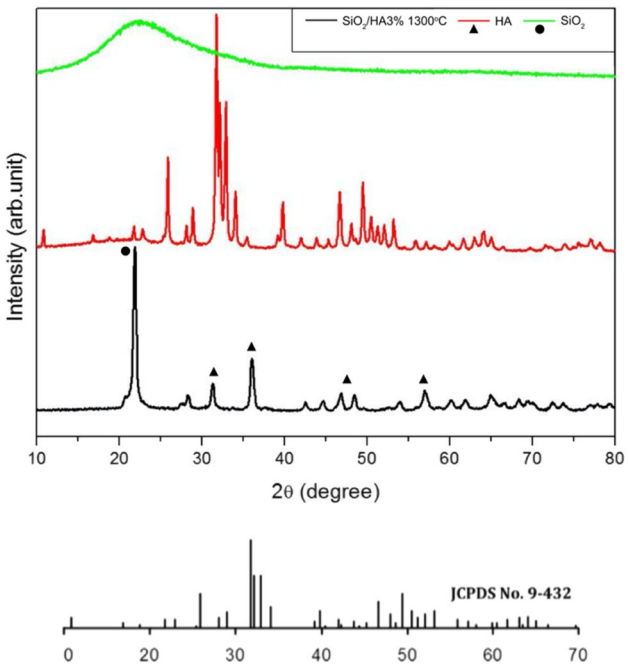

Fig. 1 XRD pattern of SiO_2, HA and SiO_2 + 3% HA (1200 °C) group. Correspond to the characteristic peak of SiO_2 (JCPDS no. 29-0085) and of HA (JCPDS no. 9-432)

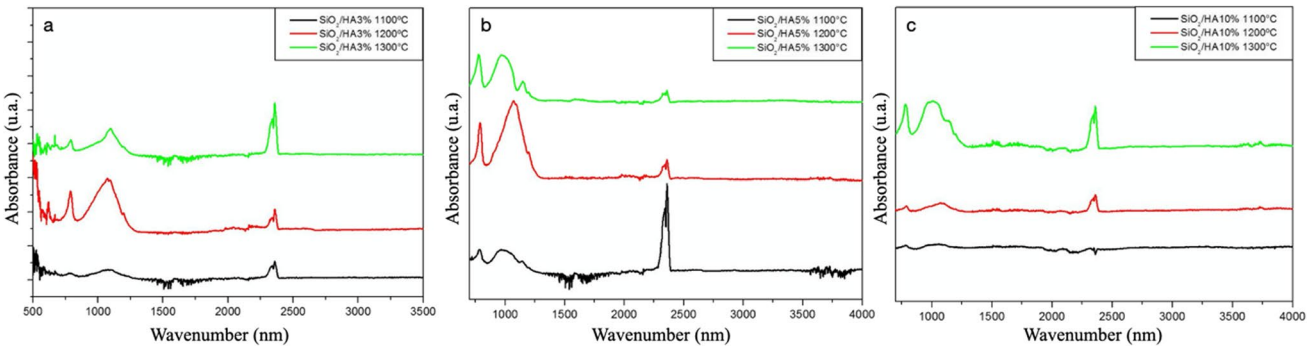

Fig. 2 FTIR pattern of SH composite ceramic in different concentration of nano-HA, 3 (**a**), 5 (**b**) and 10% (**c**), sintered at 1100, 1200 and 1300 °C

that associate SiO_2 and HA [33, 34]. The homogeneous distribution of HA nanoparticles enhances the mechanical and tribological properties acting as load carriers [35]. Increasing the proportion of HA results in a greater challenge for homogeneous distribution within the bulk, which may result in aggregated particles and the formation of mechanical deficiency regions. However, a higher concentration can provide greater bioactivity to the material [36].

In order to favor the compacting and pressing of specimens, PVB was used as a binder in this study. Definned as an amorphous thermoplastic that presents an excellent flexibility, fil-forming and adhesion, PVB acts as a cross-linked according to the number of residual OH groups presented in the material [37]. The conformation of fumed silica powder presents a great oxygen coating under ambient conditions and, although the use of binders can provide the formation of porosities in the material [38, 39], its absence could make the manipulation of the specimens unfeasible before sintering [32, 39].

3.3 Sintered SH Composite Ceramic Results

The association between uniaxial and isostatic pressing [38] combined with mechanical milling process [32] has been successfully used for the production of bioceramics with high density and mechanical behavior. These processes favored the bulk homogenization as well as the samples conformation. In this way, the material is prepared for sintering.

In this study, the plateau temperature was variated aiming to observe the reflects on physicochemical characteristics of SH composite ceramic and predict the optimal sintering scheme. Although the fusion temperature of silica is 1710 °C, further collisions result in some irreversible mechanical entanglement or agglomeration from 800 °C [40] and around 1250 – 1300 °C the compaction can occur [41]. Once the decomposition of HA initiates at 1250 – 1300 °C and reflects in grain boundaries and deterioration of mechanical properties of ceramics [42, 43], the elected temperatures were 1100, 1200 and 1300 °C to sinter the green-body specimens. Also, at temperatures above 1200º, fumed silica, glassily, affected by the presence of HA, begins a devitrification process, crystallizing and undergoing reconstructive transformations that leads to fragmentation of the material structure.

A low sintering scheme was used in order to establish a graduation of temperature favoring, i.e., the effective burn out of binder at 600 – 700 °C [44], reducing the imprisonment of CO_2 on composite ceramic body. Band at 2300 cm^{-1} could indicate these CO_2 imprisonments [45] inside the bulk of the material on FTIR analysis (Fig. 2). For concentrations of 3 and 10% HA, according to the sintering temperature, the bands of CO_2 became more prominent, while for the concentration of 5% this relationship was reversed.

Figure 3 presents the three concentration groups sintered at 1200 °C and demonstrates controlled peaks of CO_2. Spectra exhibits vibration possibly attributed to bound (3700 – 2600 cm^{-1}) and free (3571 cm^{-1}) hydroxyl stretch modes,

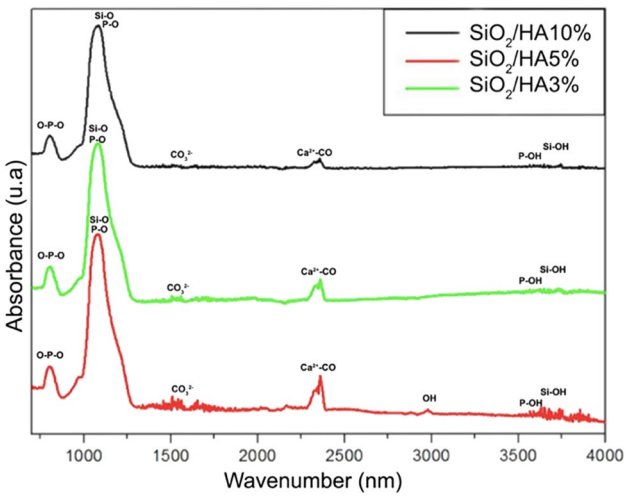

Fig. 3 FTIR pattern of SH composite ceramic sintered at 1200 °C

the carbonate asymmetric stretch (1638 cm^{-1}) and out of bending mode (875 cm^{-1}), and the phosphate asymmetric stretch (1088/1047 cm^{-1}), and v_4 O–P–O in plane bending modes at 637 cm^{-1} [34, 47]. Vibrational modes from silanol (Si–OH) stretch region stretch region (3700–2500 cm^{-1}), Si–O stretch (1100 and 962 cm^{-1}), Si–OH deformation vibration (1020 cm^{-1}) and bonded silanol groups 3400–3200 cm^{-1}, and a characteristic Si–O–Si stretch near 480 cm^{-1} did not appear in spectra, only in 1130–1000 cm^{-1} [46].

Note that HA and SiO_2 share a number of similarly spaced vibrational modes of hydroxyl stretch (3700– 2500 cm^{-1}), carbonate (1635–1640 cm^{-1}), Si–O/P–O stretch (1089–1095 cm^{-1}), Si–O/P–O symmetric stretch (958–962 cm^{-1}), and Si–O–Si stretch/P–O out of plane bending (477–483 cm^{-1}) that are not represented on Figs. 2 and 3. It could be possibly attributed due to similarities in vibrational characteristics within the SiO_4^{4-} and PO_4^{3-} tetrahedral molecular units that were possibly incorporated on the SiO_2 and HA [34].

The intensities of the weak surface P-OH vibrational mode at 3682 cm^{-1} [47], the free hydroxyl stretch at 3571 cm^{-1}, the n_3 phosphate peaks at 2100, 1088, and 1047 cm^{-1}. In addition, the carbonate n_2 mode at 875 cm^{-1} and the n_3 carbonate modes at 1638, 1455, and 1421 cm^{-1} decrease in intensity with increasing silica-coating amount.

The specimens after sintering were analyzed via XRD (Fig. 4), an interesting method to identify the phases in every group. The major peak intensity of the sintered SH at 1200 °C has a vivid increase in comparison with XRD of 1100 and 1300 °C groups. This fact indicates a increase on the powder's crystallinity. The temperature of 1100 °C presented an attempt of binding, at 1200 °C the peaks were evidenced, and at 1300 °C the degradation already prevented its increase, the HA peaks start to disappear and the formation of $Ca(OH)_2$ peaks are promoted and only tha amorphous phase of SiO_2 could be identified. The intensity of the characteristic peaks for b-tricalcium phosphate (β-TCP), located at 2θ angles of 27.75, 31.65, 45.55, and 48.00° are more prominent at 1200 °C group, temperature that would be caused the HA decomposition into α-TCP $\{Ca_3(PO_4)_2\}$, β-TCP $\{Ca_3(P_2O_8)\}$ and calcium oxide (CaO) [30].

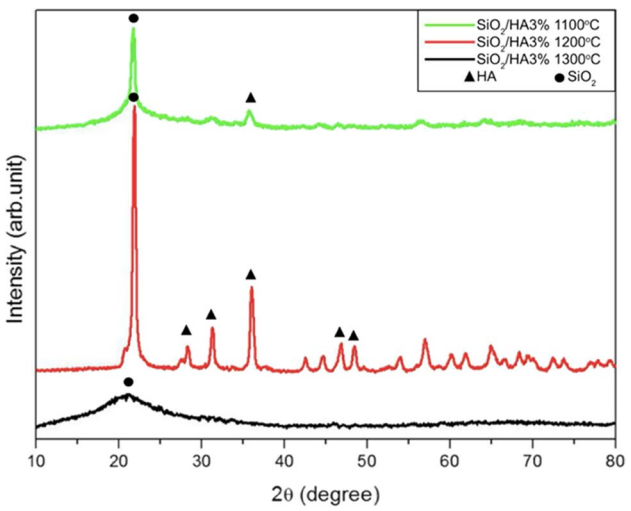

Fig. 4 XRD pattern for SH composite ceramic with 3% of HA sintered at 1100, 1200 and 1300 °C

The chemical characterization of starting powders (SiO_2, HA and SH composite ceramic blends) and after sintering was conducted using SEM/EDX. The EDX analysis detected silicon (Si) and oxygen (O), in 46.08 wt.% and 53.92 wt.%, respectively. To HA sample, EDX detected calcium (Ca) 27.38 wt.%, phosphate (P) 12.92 wt.%, carbon (C) 8.69 wt.%, sodium (Na) 0.72 wt.%, magnesium (Mg) 0.48 wt.%, and oxygen (O) 38.94 wt.%.

Aiming to characterize the effects of the sintering temperature variation, SEM was conducted on bulk area. Figure 5 instance the SH composite ceramic with 10% of HA sintered at 1100 (a, b, c), 1200 (d, e, f) and 1300 °C (g, h, i). Insufficient densification of the sample can be observed with pores and cracks in the material, functioning as potential areas to catastrophic failure during eventual mechanical challenge. Some pores can also originate from the evaporation of the PVB. At 1100 °C the flaking aspect of the agglomerated fumed silica, although compacted, continues to be observed at higher magnifications (Fig. 5b, c), in agreement with the findings of physical–chemical analysis. At temperatures of 1200 °C and 1300 °C the matrix is more homogeneous, with union of particles. However, the pores of the highest temperature appear to be of greater volume.

The starting powder of SiO_2 (Fig. 6a) demonstrates the initial appearance of flake-like with a large surface area, similar to previous description [24], and starting powder of nano-HA (Fig. 6b) showing uniformity in size, although they are agglomerated due to the high surface energy of the nanoparticles. Bends before sintering and after interaction with the alcoholic medium and homogenization with a ball mill already demonstrate a different pattern and networks of overlapping agglomerates and clusters [24, 26]. As the volume of HA increases, there is a greater dispersion and less volume of agglomeates (Fig. 6c, d, and e). The temperature chosen to demonstrate after sintering was 1200 °C as it is the average between the groups studied and help to compare the structural change that has occurred. The greater the addition of HA, the more evident the filaments within the ceramic bulk (Fig. 6h). According to EDX their composition is mostly magnesium. It was observed on the concentrations studied, but other concentrations could be investigated and a range of sintering temperature between 1200 and 1300 °C is valid to be exploited.

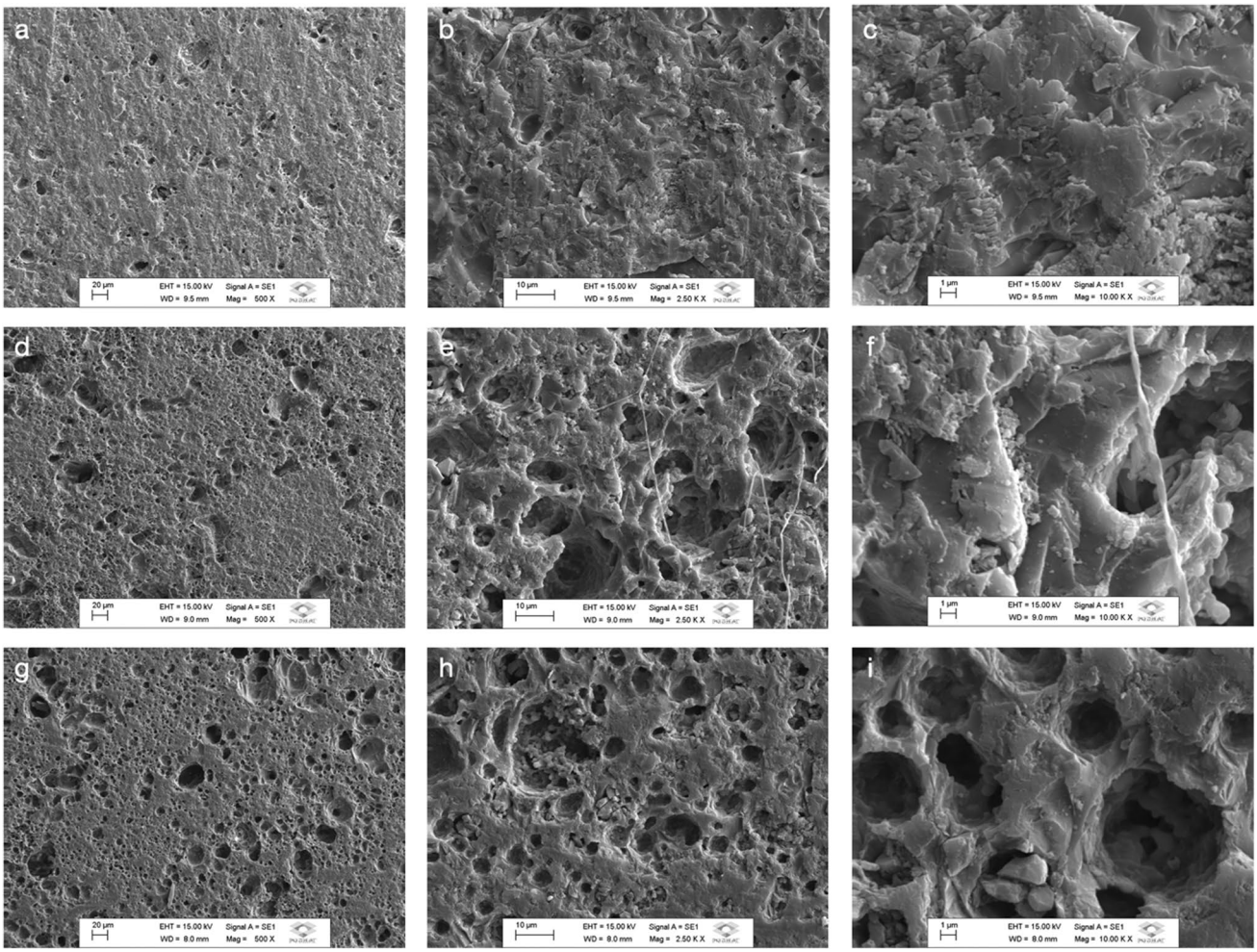

Fig. 5 SEM images of SH composite ceramic with 10% of HA sintered at 1100 (**a**, **b**, **c**), 1200 (**d**, **e**, **f**) and 1300 °C (**g**, **h**, **i**)

3.4 PVB Concentration Results

The use of a binder is essential because of the hard and limited plastic deformation capability of a ceramic powder at room temperature [48]. Lubricant, in this case the oleic acid, is used in small quantities and should not infer adhesive forces between particles. To plastically deform in between particles and transmit sufficient strength to the green compact, PVB helped to maintaining the integrity during pre-sintering handling [39]. Although, the use of organic binders requests the effective remotion in a long heating time, releasing gases that may lead the deformation of the green compact or the initiation of cracks.

PVB is usually used in necessity of a strong binding, with the ability of adhesion in different surfaces and characteristics such as toughness, flexibility and optical clarity [49]. The heat-resistance of PVB is deficient due to their low glass-transition temperature (T_g) [50]; The PVB Butvar B98 has a glass-transition temperature (Tg) between 72–78 ºC; warming up over this range will be promotes stress relief allowing handling, drilling, machining and sanding of samples, therefore, the binder performs its stabilization function and as the ceramic is sintered it will be eliminated at 600 – 700 °C [44]. Containing a hydroxyl group via polyvinyl alcohol (PVA) that dominates the adsorption on SiO_2 by hydrogen bonding, interaction already described between PVB and yttria-stabilized zirconia (YSZ) [51]. The high number of hydroxyl groups possibility more effective adsorption of PVB on the ceramic particles.

Figure 7 shows SEM images of SH composite ceramic with different concentrations of HA, sintered at 1200 °C, produced with 1.2% or 2.4 wt.% of PVB. EDX maintained the dispersion previously described and the groups with the highest concentration of PVB showed a slight increase in carbon levels. In lower magnifying, cracks can be seen in SH composite ceramic with 3% (Fig. 7a, c) and 10% (Fig. 7i) of HA, being more frequent in groups with less HA addition. The group of 10% of HA and 2.4 wt.% of PVB did not present them anymore (Fig. 7k). All groups have apparent pores, which indicates inefficiency in the compaction of

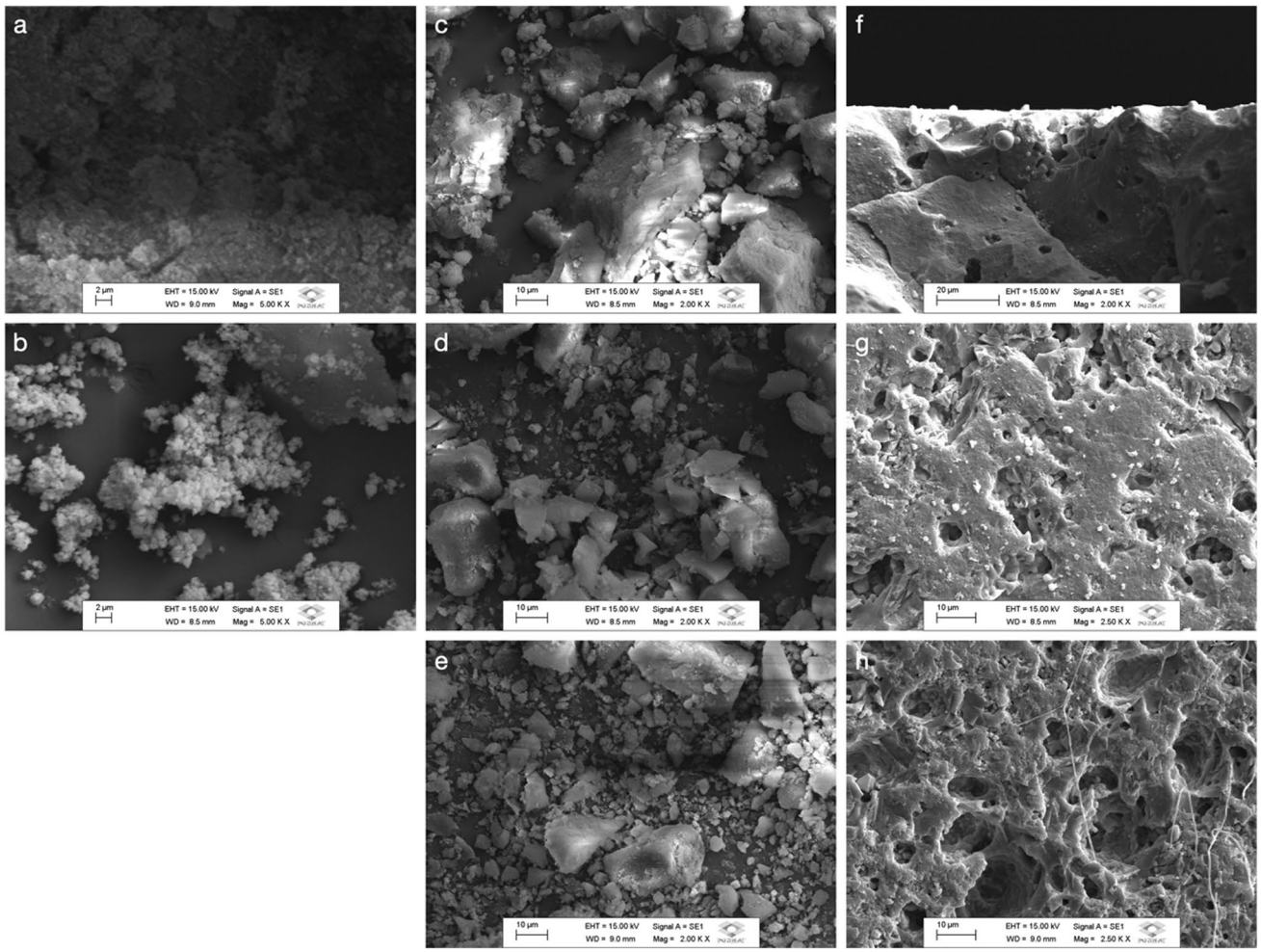

Fig. 6 SEM images of starting powder of SiO_2 (**a**), HA (**b**), SH composite ceramic with 3% of HA (**c**), 5% of HA (**d**) and 10% of HA (**e**). After sintering at 1200 °C the SH composite ceramic with 3% of HA (**f**), 5% of HA (**g**) and 10% of HA (**h**)

green body samples. Qualitatively, it can be observed that groups with 2.4 wt.% of PVB have fewer pores, which suggests more effective compaction.

XRD patterns for all samples studied are grouped at Fig. 8. SiO_2 is the predominant peak at 22° in addition to low and mean intensity peaks corresponding to $Ca_5(PO_4)_3(OH)$ and β-TCP (30 – 35°) [43], revealing that these phases tend to be maintained independent of PVB wt.% variation once de sintering temperature is the same (1200 °C). There was a maintenance of the general intensity of the spectrum, not varying significantly according to the change in concentration of the PVB, which suggests complete burn out. The volume of pores within the sample, with eventual $Ca(OH)_2$ imprisonment, should be investigated by methods such as density and pore count of the samples.

Analysis of FTIR spectra for PVB variation shows that all samples have typical absorption bands of SiO_4^{4-} at 1100, 1277, and 825 cm^{-1}. Indicating the crystalline HA, PO_4^{3-} presented bands at 1050, 961, 604, and 572 cm^{-1}, OH^- at 3574, 3440, 1630, and 634 cm^{-1}, CO_3^{2-} carbonate groups at 1550, 1457, 1415, 880, and 800 cm^{-1} (Fig. 9). It was not possible to observe changes in the spectrum in relation to the variation of the binder, between blends of starting powders and after sintering.

According to the XRD and FTIR analysis, it can be observed that the use of presence of 1.2% or 2.4 wt.% of PVB did not influence the physicochemical characteristics of the experimental material. However, it seems to have contributed to a more effective compaction of the green-body specimens, providing a lower incidence of cracks and apparent pores.

3.5 SH Composite Ceramic Results

In the present work, the nano-HA derived from bovine femurs was incorporated into a commercial fumed silica

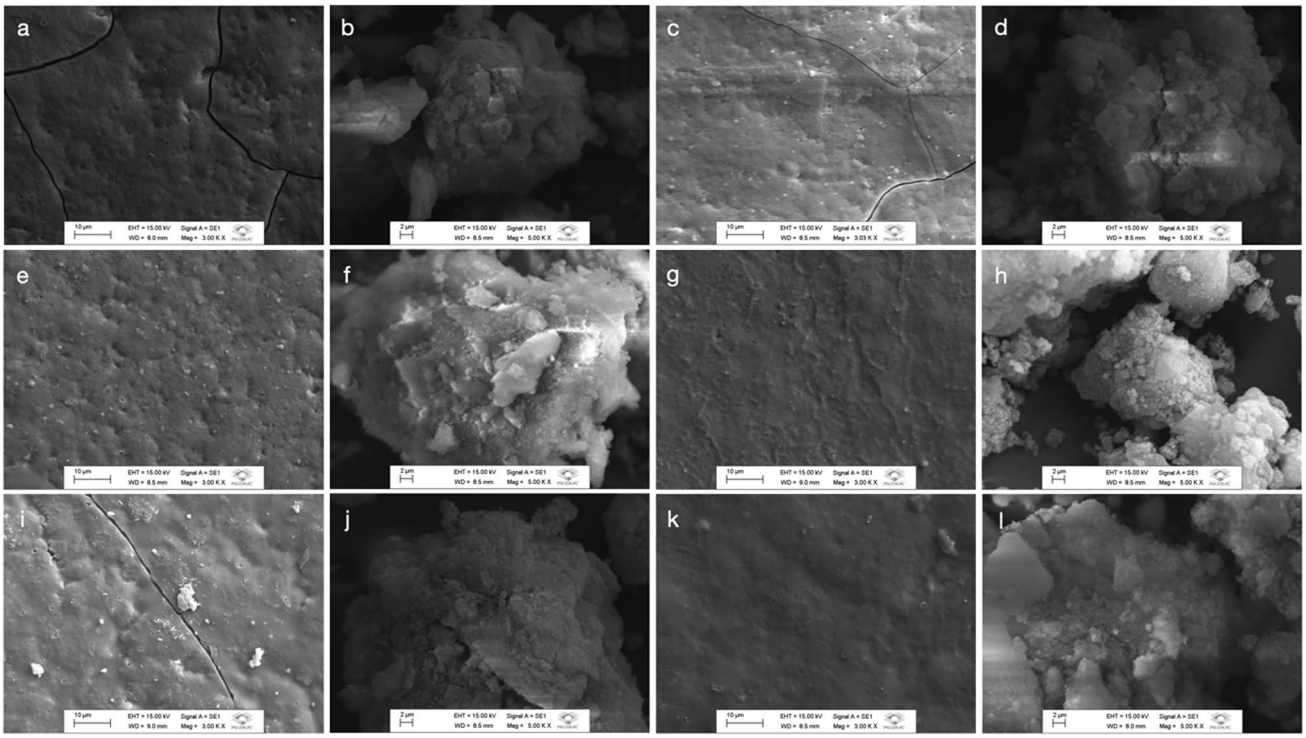

Fig. 7 SEM images of SH composite ceramic with 3% of HA 1.2% (**a**, **b**) and 2.4 wt.% of PVB (**c**, **d**), 5% of HA 1.2% (**e**, **f**) and 2.4 wt.% of PVB (**g**, **h**), and 10% of HA 1.2% (**i**, **j**) and 2.4 wt.% of PVB (**k**, **l**)

as an application of biomaterial. The study of synthesis details and characterization helped to understand the experimental material and outline future strategies to optimize it. The association between silica and HA are implemented as filled cement [35] and bone substitute material [52], due to their cell proliferation ability [53],

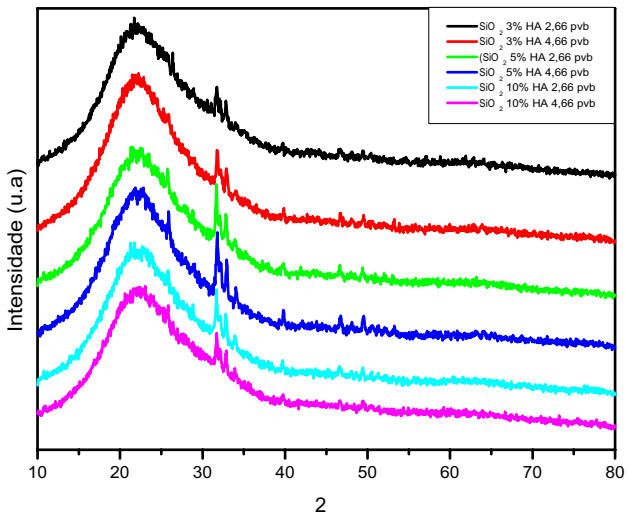

Fig. 8 XRD pattern of SH composite ceramic with different concentration of HA, varying in 1.2% and 2.4 wt.% of PVB

early bone ingrowth and repair [16], induction of an osteogenic signal to human mesenchymal stem cells [54], and biomimetic properties [52].

As described, not only the composition but also the processing technique can be responsible to physicochemical and mechanical properties of composite ceramic. It is worth noting that a porosity between 60 – 80% stimulates the osteoconductivity and biodegradability for bone substitute [55]. The characterization step is essential to guide the research line and direct the best composition and microstructural pattern for the development of subsequent tests. Critical planning and analysis will save laboratory time and financial resources.

Therefore, more investigations are needed with SH composite ceramic in order to elucidate the physicochemical, mechanical and tribological properties deepening variations and analysis of the manufacturing routes, the matrix chemical composition, different conformation of the silica particle, and the uniformization of the HA dispersion. In this way, the positive characteristics from the SH ceramic composition such as bioactivity, biocompatibility and osteoconductivity, which are widely studied, will provide the applicability of the experimental material by medical and dental community.

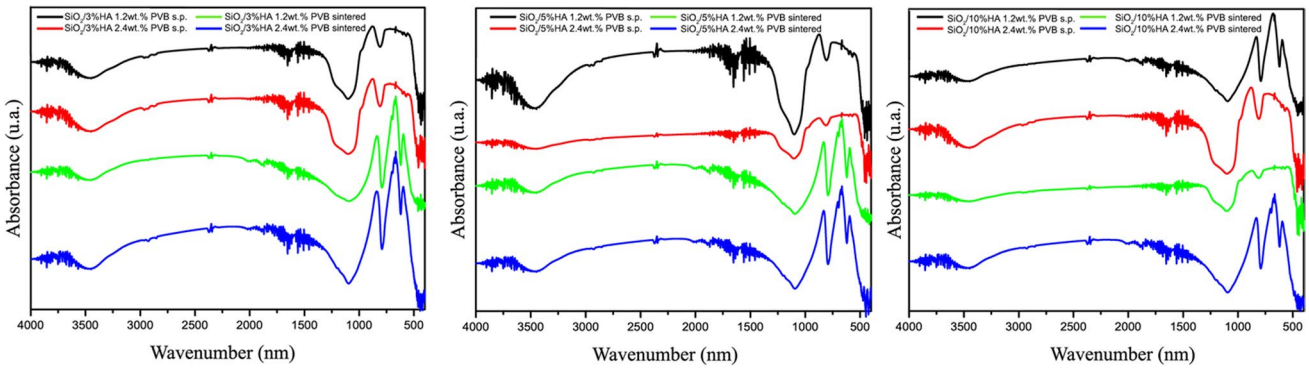

Fig. 9 FTIR pattern of SH composite ceramic. Comparison between starting powder (s.p.) and after sintering (1200 °C) varying in 1.2% and 2.4 wt.% of PVB

4 Conclusions

In the present work, a silica-hydroxyapatite composite ceramic was successfully produced and investigated according to physicochemical analysis. It was found that:

1- The nano-hydroxyapatite produced from bovine femurs was feasible for the composition of an experimental composite ceramic;
2- Based on the microstructural evolution, when sintered at 1200 °C, the chemical bonds within the material were potentialized without the degradation of hydroxyapatite on the XRD profile;
3- The composite ceramic presented no chemical changes with different concentration of PVB. However, SEM images suggests that 2.4 wt.% of PVB resulted in an of material compaction and a lower inclusion of cracks and pores. Additional methods should be performed aiming a deep evaluation;
4- The results suggested that the match composition of SiO_2 matrix with 5% of HA and 2.4 wt.% of PVB, sintered at 1200 °C, exhibit potentially superior properties to biomaterial applications.

Acknowledgements The authors are grateful for the support provided by São Paulo Research Foundation (FAPESP) and the Coordination for the Improvement of Higher Education Personnel (CAPES).

Author Contributions All authors contributed to the study conception and design. Material preparation, data collection and analysis were performed by Brunna Mota Ferrairo, Victor Mosquim, Lucas José de Azevedo-Silva, Luara Aline Pires and David Santos Souza Padovini. The first draft of the manuscript was written by Brunna Mota Ferrairo. The manuscript was revised by Aroldo Geraldo Magdalena, Carlos Alberto Fortulan, Paulo Noronha Lisboa-Filho, José Henrique Rubo and Ana Flávia Sanches Borges. All authors read and approved the final manuscript.

Funding This research was funded by São Paulo Research Foundation (FAPESP), grant number 2018/23639-0 and the Coordination for the Improvement of Higher Education Personnel (CAPES - Finance Code 001).

Data Availability All data are presented in the manuscript.

Declarations

Ethics Approval Not applicable.

Consent to Participate Not applicable.

Consent for Publication Not applicable.

Competing Interests The authors declare no competing interests.

References

1. Schwarz K, Milne DB (1972) Growth-promoting effects of silicon in rats. Nature 239:333–334
2. Jugdaohsingh R (2007) Silicon and bone health. J Nutr Health Aging 11:99–110
3. Carlisle EM (1970) Silicon: a possible factor in bone calcification. Science 167(3916):279–280
4. Botelho CM, Brooks RA, Best SM, Lopes MA, Santos JD, Rushton N, Bonfield W (2006) Human osteoblast response to silicon-substituted hydroxyapatite. J Biomed Mater Res A 79:723–730. https://doi.org/10.1002/jbm.a.30806
5. Tang Q, Brooks R, Rushton N, Best S (2010) Production and characterization of HA and SiHA coatings. J Mater Sci Mater Med 21:173–181. https://doi.org/10.1007/s10856-009-3841-y
6. Gao T, Aro HT, Ylänen H, Vuorio E (2001) Silica-based bioactive glasses modulate expression of bone morphogenetic protein-2 mrna in saos-2 osteoblasts in vitro. Biomaterials 22:1475–1483
7. Patel N, Best SM, Bonfield W, Gibson IR, Hing KA, Damien E, Revell PAA (2002) Comparative study on the in vivo behavior of hydroxyapatite and silicon substituted hydroxyapatite granules. J Mater Sci Mater Med 13:1199–1206. https://doi.org/10.1023/a:1021114710076

8. Sadat-Shojai M, Khorasani MT, Dinpanah-Khoshdargi E, Jamshidi A (2013) Synthesis methods for nanosized hydroxyapatite with diverse structures. Acta Biomater 9:7591–7621
9. Mohd Pu'ad NAS, Koshy P, Abdullah HZ, Idris MI, Lee TC (2019) Syntheses of hydroxyapatite from natural sources. Heliyon 5:e01588
10. Gibson IR, Best SM, Bonfield W (1999) Chemical characterization of silicon-substituted hydroxyapatite. J Biomed Mater Res 44:422–428. https://doi.org/10.1002/(sici)1097-4636(19990315)44:4%3c422::aid-jbm8%3e3.0.co;2-#
11. Coathup MJ, Samizadeh S, Fang YS, Buckland T, Hing KA, Blunn GW (2011) The osteoinductivity of silicate-substituted calcium phosphate. J Bone Joint Surg Am 93A:2219–2226. https://doi.org/10.2106/Jbjs.J.01623
12. Wiens M, Bausen M, Natalio F, Link T, Schlossmacher U, Muller WE (2009) The role of the silicatein-alpha interactor silintaphin-1 in biomimetic biomineralization. Biomaterials 30:1648–1656. https://doi.org/10.1016/j.biomaterials.2008.12.021
13. Botelho CM, Lopes MA, Gibson IR, Best SM, Santos JD (2002) Structural analysis of Si-substituted hydroxyapatite: zeta potential and X-ray photoelectron spectroscopy. J Mater Sci Mater Med 13:1123–1127
14. Kalia P, Brooks RA, Kinrade SD, Morgan DJ, Brown AP, Rushton N, Judjaohsingh R (2016) Adsorption of amorphous silica nanoparticles onto hydroxyapatite surfaces differentially alters surfaces properties and adhesion of human osteoblast cells. PLoS ONE 11:e0144780. https://doi.org/10.1371/journal.pone.0144780
15. Borden M, Attawia M, Khan Y, Laurencin CT (2002) Tissue engineered microsphere-based matrices for bone repair: design and evaluation. Biomaterials 23:551–559
16. Hing KA, Revell PA, Smith N, Buckland T (2006) Effect of silicon level on rate, quality and progression of bone healing within silicate-substituted porous hydroxyapatite scaffolds. Biomaterials 27:5014–5026
17. Sych EE, Pinchuk ND, Klimenko VP, Uvarova IV, Tovstonog AB, Tomila TV, Evich YI (2015) Synthesis and properties of Si-modified biogenic hydroxyapatite ceramics. Powder Metall Met Ceram 54:67–73. https://doi.org/10.1007/s11106-015-9681-z
18. Tolouei R, Tan CY, Ramesh S, Sopyan I, Teng WD (2011) Effect of nano silica on the sinterability of hydroxyapatite dense bodies. Adv Mater Res 264–264:1832–1838
19. Turner IG (2009) Ceramics and glasses. In: Narayanan R (ed) Biomedical materials. Springer, New York, pp 3–39
20. Bowen P, Carry C (2002) From powders to sintered pieces, forming, transformations and sintering of nanostructured ceramic oxides. Powder Technol 128:248–255
21. Vallet-Regí M, Ragel CV, Salinas AJ (2003) Glasses with medical applications. Eur J Inorg Chem 6:1029–1042
22. Gorustovich A, Roether J, Boccaccini AR (2010) Effect of bioactive glasses on angiogenesis: in-vitro and in-vivo evidence. Tissue Eng B Rev 16:199–207
23. Ferrairo BM, Mosquim V, de Azevedo-Silva LJ, Pires LA, Padovini DSS, Magdalena AG, Fortulan CA, Rubo JH, Borges AFS (2023) Production of bovine hydroxyapatite nanoparticles as a promising biomaterial via mechanochemical and sonochemical methods. Mater Chem Phys 295:127046. https://doi.org/10.1016/j.matchemphys.2022.127046
24. Srinivasa RR, Saad AK (1997) Shear-thickening response of fumed silica suspensions under steady and oscillatory shear. J Colloid Interf Sci 185:57–67
25. Whitby CP, Krebsz M, Booty SJ (2018) Understanding the role of hydrogen bonding in the aggregation of fumed silica particles in triglyceride solvents. J Colloid Int Sci 527:1–9
26. Reghavan SR, Khan SA (1995) Shear-induced microstructural changes in flocculated suspensions of fumed silica. J Rheol 39:1311–1325. https://doi.org/10.1122/1.550638
27. Yziquel F, Carreu PJ, Tanguy PA (1999) Non-linear viscoelastic behavior of fumed silica suspensions. Rheol Acta 38:14–25
28. Herliansyah MK, Nasution DA, Hamdi M, Ide-Ektessabi A, Wildan MW, Tontowi AE (2007) Preparation and characterization of natural hydroxyapatite: a comparative study of bovine bone hydroxyapatite and hydroxyapatite from calcite. Mater Sci Forum 561–565:1441–1444
29. Ooi C, Hamdi M, Ramesh S (2007) Properties of hydroxyapatite produced by annealing of bovine bone. Ceram Int 33:1171–1177
30. Kothapalli C, Wei M, Vasiliev A, Shaw MT (2004) Influence of temperature and concentration on the sintering behavior and mechanical properties of hydroxyapatite. Acta Mater 52:5655–5663
31. Boskey A, Camacho NP (2007) FT-IR imaging of native and tissue engineered bone and cartilage. Biomaterials 28:2456–2478
32. Mosquim V, Ferrairo BM, Vertuan M, Magdalena AG, Fortulan CA, Lisboa-Filho PN, Cesar PF, Bonfante EA, Honório HM, Sanches Borges AF (2020) Structural, chemical and optical characterizations of an experimental SiO2-Y-TZP ceramic produced by the uniaxial/isostatic pressing technique. J Mech Behav Biomed Mater 106:103749. https://doi.org/10.1016/j.jmbbm.2020.103749
33. Kelly JR, Benetti P (2011) Ceramic materials in dentistry: historical evolution and current practice. Aust Dent J 56:84–96. https://doi.org/10.1111/j.1834-7819.2010.01299.x
34. Borum L, Wilson Jr OC (2003) Surface modification of hydroxyapatite. Part II. Silica. Biomaterials 24:3681–3688. https://doi.org/10.1016/s0142-9612(03)00240-0
35. Ayatollahi MR, Yahya MY, Shirazi HA, Hassan SA (2015) Mechanical and tribological properties of hydroxyapatite nanoparticles extracted from natural bovine bone and the bone cement developed by nano-sized bovine hydroxyapatite filler. Ceram Int 41:10818–10827
36. Hench LL, Wilson J (1984) Surface-active biomaterials. Science 226:630–636. https://doi.org/10.1126/science.6093253
37. Polymer Properties Database. Available online: polymerdatabase.com. Acessed 15 January 2020
38. Jiang L, Liao Y, Wan Q, Li W (2011) Effects of sintering temperature and particle size on the translucency of zirconium dioxide dental ceramic. J Mater Sci Mater Med 22:2429–2435. https://doi.org/10.1007/s10856-011-4438-9
39. Pizette P, Martin CL, Delette G, Sans F, Geneves T (2013) Green strength of binder-free ceramics. J Eur Ceram Soc 33:975–984. https://doi.org/10.1016/j.jeurceramsoc.2012.11.018
40. Sigma-Aldrich Product Information (2012) Silica, Fumed. Sigma-Aldrich Co.
41. Barraclough KG, Loni A, Caffull E, Canham LT (2007) Cold compaction of silicon powders without a binding agent. Mater Lett 61:485–487. https://doi.org/10.1016/j.matlet.2006.04.102
42. Royer A, Viguie J, Heughebaert M, Heughebaert J (1993) Stoichiometry of hydroxyapatite: influence on the flexural strength. J Mater Sci Mater Med 4:76–82
43. Wang PE, Chaki T (1993) Sintering behaviour and mechanical properties of hydroxyapatite and dicalcium phosphate. J Mater Sci Mater Med 4:150–158
44. Baklouti S, Bouaziz J, Chartier T, Baumard J (2001) Binder burnout and evolution of the mechanical strength of dry-pressed ceramics containing poly(vinyl acohol). J Eur Ceram Soc 21:1087–1092. https://doi.org/10.1016/S0955-2219(00)00305-8
45. Sanati M, Andersson A (1993) DRIFT study of the oxidation and the ammoxidation of toluene over a TiO2 (B) -supported vanadia catalyst. J Mol Catal 81:51–62. https://doi.org/10.1016/0304-5102(93)80022-M

46. Socrates G (2001) Infrared and Raman characteristic group frequencies: tables and charts, 3rd edn. Wiley, New York, pp 229–246
47. Ishikawa T, Wakamura M, Kondo S (1989) Surface characterization of calcium hydroxyapatite by Fourier transform infrared spectroscopy. Langmuir 5:140–144
48. Szepesi CJ, Cantonnet J, Kimel RA, Adair JH (2011) A critical assessment of nanometer scale zirconia green body formation by pressure filtration and uniaxial compaction. J Am Ceram Soc 94:4200–4206
49. Dhaliwal AK, Hay JN (2002) The characterization of polyvinyl butyral by thermal analysis. Thermochim Acta 391:245–255. https://doi.org/10.1016/S0040-6031(02)00187-9
50. El-Din NMS, Sabaa MW (1995) Polym Degrad Stabil 47:283
51. Kuscer D, Bakarič T, Kozlevčar B, Kosec M (2013) Interactions between lead-zirconate titanate, polyacrylic acid, and polyvinyl butyral in ethanol and their influence on electrophoretic deposition behavior. J Phys Chem B 117:1651–1659. https://doi.org/10.1021/jp305289u
52. Kruse A, Jung RE, Nicholls F, Zwahlen RA, Hämmerle CHF, Weber FE (2011) Bone regeneration in the presence of a synthetic hydroxyapatite/silica oxide -based and a xenogenic hydroxyapatite -based bone substitute material. Clin Oral Impl Res 22:506–511. https://doi.org/10.1111/j.1600-0501.2010.02039.x
53. Xu JL, Khor KA (2007) Chemical analysis of silica doped hydroxyapatite biomaterials consolidated by a spark plasma sintering method. J Inorg Biochem 101:187–195
54. Huang DM, Chung TH, Hung Y, Lu F, Wu SH, Mou CY, Yao M, Chen YC (2008) Internalization of mesoporous silica nanoparticles induces transient but not sufficient osteogenic signals in human mesenchymal stem cells. Toxicol Appl Pharmacol 231:208–215
55. Werner J, Linner-Krcmar B, Friess W, Greil P (2002) Mechanical properties and in vitro cell compatibility of hydroxyapatite ceramics with graded pore structure. Biomaterials 23:4285–4294